Full Length Article

Structure and electronic properties of tin monoxide (SnO) and lithiated SnO terminated diamond (1 0 0) and its comparison with lithium oxide terminated diamond

Sami Ullah [a,b,*], Gary Wan [a,b], Christos Kouzios [a,b], Cameron Woodgate [a,b], Mattia Cattelan [c], Neil Fox [a,c]

[a] School of Physics, HH Wills Physics Laboratory, University of Bristol, Tyndall Avenue, Bristol BS8 1TL, United Kingdom
[b] Bristol Centre for Functional Nanomaterials, University of Bristol, Tyndall Avenue, Bristol BS8 1TL, United Kingdom
[c] School of Chemistry, Cantocks Close, Bristol BS8 1TS, United Kingdom

ABSTRACT

Wideband gap diamond-based materials are attracting huge interest for energy harvesting and quantum applications. We have used density functional theory code (DFT) to explore tin (Sn) as a potential negative electron affinity (NEA) imparting termination on the oxygen terminated diamond (OTD) surface. Large adsorption energies ($\sim$−6 eV) were obtained for half monolayer of Sn atoms on oxygen (O) terminated diamond surface with an NEA of up to −1.37 eV. We are also demonstrating experimentally, the formation of SnO nano cluster layer on the surface of diamond which resulted in NEA and reduction in the work function (WF) by 1.8 eV. The SnO termination, clearly distinguishable from more stable and widely known SnO_2, was found to be stable in ambient conditions, a crucial point for device application. A comparison of lithium (Li) and Li/Sn oxide terminations of single crystal diamond (1 0 0) is presented in terms of the stability of the surface layer and the electronic properties thus induced, using the photoemission spectroscopic techniques. The intercalation of Li into SnO planes results in the increased stability of LiO on the surface of diamond and WF reduction by 2.3 eV which paves way for a more efficient termination on the diamond surface.

1. Introduction

Diamond is used in thermionic emission and field emission devices among others in electron sources, energy harvesting devices and radiation converters etc. [1–3]. Diamond can pave a novel way in energy sector in the form of renewal of renewable energy sources. One of the most interesting properties of diamond is the negative electron affinity (NEA) which means that the vacuum level lies below the conduction band, which makes diamond an efficient source of electrons [4–9]. The NEA can appear when the surface carbon atoms are negatively charged which has been achieved by terminating the diamond surface suitably. Hydrogen termination has been demonstrated to impart a NEA value of −1.3 eV measured experimentally to the diamond surface [8,10,11]. However, besides being widely studied, hydrogen terminated diamond surface suffers from the problem of instability due to hydrogen desorption at higher temperatures [11]. When either H desorbs or is replaced by O, the NEA character is lost. Another problem with

hydrogen terminated surfaces is water adsorption on H-terminated surfaces which leads to charge transfer and hence upward band bending [12,13] which again causes loss of NEA. As an alternative, a monolayer or sub monolayer coverage of some of the electropositive group I and II metals [14–17] and first row transition metals (TMs) [18–22] on the bare and oxygen terminated diamond surface have been found to be a suitable candidate for diamond surface termination. Transition metals like Cu, Ti, Ni and Co metals have been found theoretically to impart NEA to the diamond surface however their ability to do so depends upon their capacity to form a carbide on the diamond surface in which only Ti and V have been able to show higher NEA value than others [23,24]. Most of these metals, however, do not form a stable monovalent bond with carbon which was solved by using an oxygen terminated diamond (OTD) surface instead of a bare diamond surface. The key here is to induce stronger bonding between the metal layer and the underlying diamond surface and hence a large surface dipole. Alkali metals like Na, K and Li have been explored as potential terminations on diamond

surfaces. Petrick and Bennedorf found a much higher sticking coefficient and hence a prospect of stronger bonding of K on oxygen terminated diamond than on hydrogen terminated diamond [25]. In other words metal oxygen and carbon oxygen bonds have been found to be stronger and highly stable than metal carbon bonds [26,27]. James [28] has theoretically demonstrated Al termination of 1 ML on the surface of diamond with an adsorption energy (E_a) value of −4.11 eV and NEA of −1.47 eV. A larger value of adsorption energy (E_a), −5.24 eV with an NEA of −1.36 eV, was obtained with Al termination of 0.25 ML on the OTD. Cs-O terminated diamond surface has been found to possess a very low WF of ~1.5 eV but despite this it is highly unstable due to the loss of Cs above 400 °C [14]. Stable low WF surfaces in thermionic emission devices are required to work at higher temperatures. O'Donnell [29] have been able to demonstrate air stable lithium (Li)-O terminated NEA diamond surface successfully with controlled atomic layer coverage and stability at 800 °C. However, we have found in our study that Li desorbs at 800 °C along with most of the oxygen from the diamond surface, which leads us to develop a method to increase the stability of Li on the surface of diamond. Such method is to explore a suitable metallic termination on the diamond surfaces which can render Li adsorption on the surface of diamond more stable at higher temperatures and help in decreasing the WF further for thermionic emission.

Recently, the formation of Si and Ge terminated diamond surfaces have also been investigated. Schenk [30,31] has demonstrated the Si terminated diamond (1 0 0) surface with a two domain 3 × 1 reconstruction. This has resulted in an NEA of 0.86 ± 0.1 eV. However, Si terminated diamond is unsuitable for the ambient environment due to its high reactivity and any application in the atmospheric environment would need a protective SiO_2 coating on the top. A similar structure has been obtained with Ge terminated diamond with a maximum coverage of 0.63 ML which has resulted in an NEA of 0.71 eV as shown by Sear [32]. A novel termination that we explore in this paper is tin (Sn), a same group element with C, Si and Ge, that has been ignored as a potential candidate for the studies on metal and metal oxide termination on the diamond surface. As a known fact tin monoxide (SnO) is a capable and promising p-type semiconductor with an experimental, small indirect bandgap of 0.7 eV [33] and a direct energy gap that ranges from 2.5 to 3 eV [34], Sn is abundantly available with non-toxic nature. Sn vacancy has been found to be the main source of p-type nature of SnO which can be altered by proper doping. On top of that Sn, alloyed with alkali metals (Li, Na, etc.) in a specific stoichiometric ratio has been found to possess ultra-low work function (WF) in bulk form e.g. a stoichiometric alloy of Sn2Li5 has been found to possess a WF of 1.25 eV [35].

Oxide-based 2D materials have been found to be dynamically stable and less susceptible to degradation in air [36,37]. Li intercalation into tin oxide (SnO_x) as an active electrode material for metal ion batteries has been widely studied in theory and experiment [38–40]. It has been found that lithiation of pristine SnO layers results in the formation of stable layered Li_xO structure. The expelled Sn atoms form atomic planes to separate the Li_xO layers [41]. The formation of such stable structures on the surface of diamond and the interaction of SnO_x with the diamond surface carbon atoms would be an interesting area to investigate with the purpose to demonstrate a highly stable and high temperature resistant, NEA imparting termination on the surface of diamond.

In this paper, we are exploring the possibility of Sn as a stable and efficient NEA imparting termination on the surface of oxygen terminated diamond (1 0 0) using the density functional theory (DFT) code. We are also demonstrating the formation of stable SnO on the surface of diamond (1 0 0) surface, reliably, by Physical Vapour Deposition (PVD) technique, shedding light on heavy metal oxide terminations and their effect on electron affinity. Reliably, forming a stable layer of SnO and discerning it from the SnO_2 (a widely studied and more stable form of tin oxide) has been deemed as one of the unfulfilled goals in this aspect of material research as the surety of obtaining a phase pure SnO has been lacking due to non-availability of a reference. Using the same technique, the Li is deposited and its interaction with SnO is investigated. Through

a range of surface science techniques, we have characterised the formation of SnO and SnO_x/Li_2O termination on the surface of diamond. We show that Li_2O termination, which has been found to impart NEA, is less stable that SnO_x/Li_2O terminated diamond at high temperatures. The electron yield, though in the case of Li—O is higher than SnO_x/Li_2O terminated diamond, decreases more rapidly in Li—O with the high annealing temperature. These positive points beckon towards the increased stability of SnO_x/Li_2O terminated diamond and drive the interest in this exploration.

2. Methods

2.1. Density functional theory modelling

DFT Modelling was done using the Perdew–Burke–Ernzerhof (PBE) approximation[42] to study various configurations of Sn on oxygen terminated diamond (1 0 0) with the Cambridge Serial Total Energy Package (CASTEP)[43]. The electron density was constructed using a plane wave basis set with a cut off energy of 700 eV [44]. A symmetrical 12-carbon layer diamond slab with a 2 × 2 supercell yielding 4C atoms on the surface, enabled us to vary the coverage of Sn from quarter (QML = 1 Sn atom), to half (HML = 2 Sn atoms) to full monolayer (FML = 4 Sn atoms). For (1 0 0) surface, a supercell of dimensions 5.016 Å × 5.016 Å × 35.7 Å was used and a Monkhorst and Pack (MP) grid of 6 × 6 × 1 k-points was observed to be sufficient to sample the Brillouin zone for energy minimisation steps [45]. The calculations were performed as described by James [28].

2.2. Diamond preparation

High Pressure High Temperature (HPHT) boron doped single crystal diamonds (purchased from Element Six (145-500-0248 and MM 111/4010) with a boron doped layer on top was used in this experiment. Boron doped layer was grown in hot filament chemical vapor deposition reactor using a gas mixture comprising H_2, CH_4 (both Air Liquide, Ltd) at a flow rate of 200 and 2 standard cubic centimetres per minute (sccm), respectively, i.e. 1% CH_4 in H_2 and 5% B_2H_6 in H_2 (BOC Group, plc) with a flow rate of 0.1 sccm for epitaxial B-doped layers on single crystal diamond. The treatment was carried out for 60 min at a pressure of 20 Torr and a temperature of ~2300 K which enables a deposition of a good quality diamond thin film at a growth rate of ~0.5 μm h^{-1}. BDD overlayers grown in the same reactor under the same conditions has previously been shown to contain a boron concentration of up to ~10^{20} cm^{-3}, measured from a depth profile using secondary ion mass spectroscopy [46]. The cleaning of the sample surface along with hydrogen termination was done by microwave plasma method using a pure hydrogen plasma at 900 °C for 2 min, followed by another 2 min at 500 °C as described in [8]. The samples were treated with ozone for 30 min to render it O-terminated which was later made evident by XPS analysis.

2.3. Ultra-high vacuum techniques

The film deposition and analysis of the sample were carried out completely under Ultra-high Vacuum (UHV) conditions in interconnected chambers.

Before starting any analysis or deposition, samples were cleaned by annealing the sample at a temperature of 300 °C for 60 min under UHV conditions to remove water and adventurous carbon contamination [47].

2.4. Thin film deposition

Sn metal deposition was achieved by e-beam deposition. Tin granules were evaporated from a molybdenum crucible. The thickness calibration was optimized by a quartz micro-balance. 0.8 ML of tin was deposited at a temperature (substrate) of 327 °C on the surface of

diamond (1 0 0).

Li deposition was achieved using a thermal evaporator which consisted of a boron-nitride crucible resistively heated by a tungsten filament. A thermocouple was present in the evaporator to monitor crucible temperature. The crucible deposition temperature was set to 410 °C.

Molecular oxygen dosing was performed at an oxygen pressure of 1.5×10^{-6} mbar. Atomic oxygen dosing was achieved by dosing O_2 trough a gas cracker at 1.5×10^{-6} mbar.

2.5. Analysis methods

A series of surface analysis was performed at each step of the sample preparation, i.e. X-ray photoelectron spectroscopy (XPS), Spot profile analysis – Low energy electron diffraction SPA-LEED, Ultra violet photoelectron spectroscopy (UPS), Work Function (WF) maps, Angle resolved photoemission spectroscopy (ARPES).

XPS was carried out using a monochromatic Al K_α source (1486.7 eV) and the electron analyser at 45° to the sample normal.

SPA-LEED was used with electrons at 100 eV to investigate the surface roughness and reconstructions.

UPS and full wave vector ARPES were carried out using monochromatized He I and He II sources with energy of 21.2 eV and 40.8 eV, respectively. WF mapping was done using a non-monochromatic mercury (Hg) lamp source of $\approx$5.2 eV. WF maps of the samples were generated from fitting EF-PEEM images close to the WF cut-off edge, using a pixel-by-pixel sigmoid fit. The lateral resolution of the WF map was less than 150 nm.

3. Results and discussion

The results from the DFT calculations are presented here to support the XPS and WF data on SnO terminated diamond. We also present here the XPS and UPS data for Li—O-terminated diamond and compare it with SnO-terminated and SnO_x/Li_2O-terminated Diamond surface. The differently terminated surfaces will present different photoemission properties with Li—O-terminated diamond already known to possess NEA [29,48] while SnO terminated diamond and SnO_x/Li_2O terminated diamond will be a new exploration.

3.1. LiO_x-terminated diamond

Li was deposited on oxygen terminated single crystal diamond (B-doped C(1 0 0)-(1 × 1):O) [49] in different conditions, at room temperature and subsequently annealed at 500 and 800 °C. Quantitative XPS information shown in Table 1 shows that the Area % of Li was reduced by the 60 min 500 °C annealing, and completely removed by a 15 min 800 °C anneal. Oxygen was also largely removed at 800 °C, indicating that the carbon–oxygen bonds were broken rather than the

Table 1
Quantitative XPS survey peak information showing that the amount of Li is reduced by the 500 °C anneal and removed by the 800 °C anneal.

Sample	Peak	Area %
Pre Li	O 1s	6.4
	C 1s	93.6
	Li 1s	–
Li Deposited	O 1s	8.67
	C 1s	80.35
	Li 1s	10.98
500 °C Anneal	O 1s	5.26
	C 1s	87.88
	Li 1s	6.68
800 °C Anneal	O 1s	0.51
	C 1s	99.49
	Li 1s	–

Li—O bonding due to a small amount of oxygen remaining with no detectable Li remaining.

To understand the process of O—Li adsorption and removal with annealing temperature on the surface of diamond, component analysis of the oxygen peak is shown in Fig. S1. A component at low binding energy is linked to the O—Li peak in Fig. S1b. The component became the most relevant after annealing at 500 °C implying that the lithium is distributed on the surface, however SPA-LEED acquisition (Fig. S3) shows no new visible reconstruction other than the same B-doped C (1 0 0)-(1 × 1):O, which could mean a (1 × 1) reconstruction or amorphous layer on the surface which is counter-intuitive as Li has been found to form (2 × 1) reconstruction on the surface of Diamond (1 0 0) [48,29].

With 500 °C annealing the component peaks shift towards the higher binding energies with a large apparent O—Li component at 530.9 eV [50] while Li is at 56 eV [51]. During the annealing, heating evolves 'bulk' lithium with a different bond energy to Li—O, perhaps approaching a sub-monolayer, evidence of which can be seen in the reduction of Li peak intensity and area in Fig. S1e.

3.2. SnO terminated surface

In order to analyse the SnO_x/Li_2O terminated diamond structure, first we analyse the formation of SnO on the surface of diamond. DFT calculations revealed the suitable configurations of Sn on OTD. It was seen that Sn produces NEA on the surface of OTD (1 0 0) in nearly all configurations. Larger adsorption energies were obtained at QML (0.25 ML) and HML (0.5 ML) of Sn on oxygen terminated diamond (both ether and ketone of oxygen termination were considered). Sn was seen to prefer a position on top of oxygen rather than in between the two oxygen atoms. A very low adsorption energy was obtained with the FML (1 ML) of Sn on diamond which could be because of the large size of Sn atoms and increased electrostatic repulsion between them, hence no bonding occurring between the Sn atoms and the surface C atoms of diamond. The two most stable configurations of Sn in QML and HML configuration can be seen in Fig. 1. An NEA of −1.37 eV was obtained with an E_a of −6.03 eV at HML of Sn on top of carbonyl oxygen atoms while an electron affinity (EA) of 0.16 eV with an E_a of −6.45 eV was obtained for QML of Sn in the same configuration. However, for a QML of Sn i.e., 1 Sn atom, on top of OTD (ether terminated), an NEA value of −0.86 eV was obtained with an E_a of −5.9 eV.

3.3. Deposition of Sn on OTD

Sn was deposited at a temperature of 327 °C on the surface of OTD (1 0 0) which is slightly higher than the melting point of Sn. A quartz microbalance was used to optimise the sub monolayer deposition of Sn on the surface of B-doped C(1 0 0)-(1 × 1):O.

Initially after the deposition, a metallic peak of Sn was observed at a lower binding energy of 484.9 eV [52] along with an oxide peak at a higher binding energy of 485.5 eV[53]. The presence of the two peaks implies partial oxidation of thin sub monolayer Sn film or clusters to form SnO nanocluster (oxides) on the surface of diamond (1 0 0) as Sn has been shown to form nano-oxides on the surface of other substrates e. g. Pt [54] in different patterns. The ideal case in our study would be to form a continuous layer of SnO on the surface of diamond.

The sample was initially annealed at 600 °C for 60 min without any significant change in the film. Atomic oxygen exposure was found to be the most effective method in our experiments to transform metallic Sn into SnO than the molecular oxygen exposure. The sample was exposed to the atomic oxygen (oxygen cracking) for 70 min at a pressure of $\sim10^{-6}$ mbar at the room temperature (RT) and then annealed at 500 °C for 60 min again. As can be seen in Fig. 2, the presence of an O 1 s component at lower binding energy along with the Sn 3d oxide peak confirms the controlled formation of SnO termination on the surface of diamond, while another oxygen vacancy peak at slightly higher binding
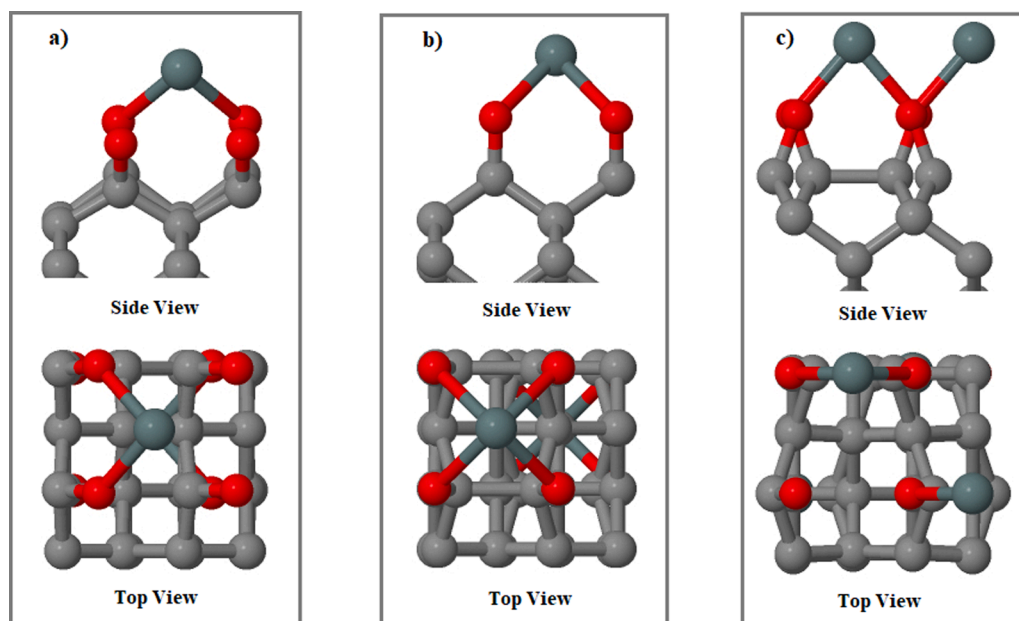
Fig. 1. Geometry optimised output structures showing (a) QML (1 atom) of Sn on the oxygen (ether) terminated diamond which has resulted in no surface reconstruction. (b) QML (1 atom) Sn on the oxygen (ketone/carbonyl) terminated diamond; the breaking of ketone bond has resulted in the surface reconstruction between the C atoms. (c) HML where 1 Sn is in between the two O (ketone) atoms hence resulted in reconstruction (or C—C bond) on the surface whereas the other Sn atom in on top of another O atom. All of these configuration show NEA with a large E_a.
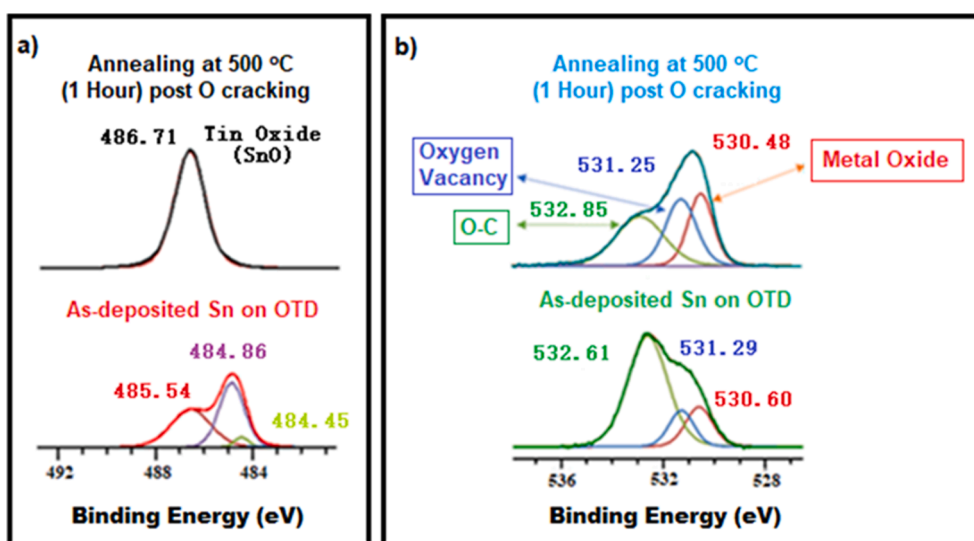

Fig. 2. XPS of the sample at each process step showing (a) Transition of Sn from metallic and oxide combination to pure oxide phase using oxygen cracking and annealing. (b) Change in Oxygen peaks during the process. We have a peak for metal oxide (SnO) and an oxygen vacancy peak at 530.5 eV and 531.3 eV[55].

energy has been reported by Park et al. [55]. We believe that we have been able to form SnO rather than SnO_2 on the diamond (1 0 0) due to the presence of Sn4d spin orbit doublet and the fact that any further process (Li deposition and annealing in our case) results in the Sn4d spin orbit doublet retaining its shape for SnO adsorbed layers as can be seen in Fig. S6, while as it transforms into a 4 peak structure for SnO_2 [56]. These results could serve as a reliable reference for SnO which has been lacking ever since. Molecular oxygen was used to oxidise the sample along with annealing at a temperature of 600 °C for 60 min, however it did not show any significant change. This finding indicates that atmospheric conditions probably will not have a significant effect on the SnO termination on the surface of diamond which indicates increased stability of the termination in the ambient conditions. Stability is a necessary condition for application in device fabrication outside the UHV environment.

The SPA-LEED data (Fig. S4) proves that the (1 × 1) reconstruction of the diamond (1 0 0) is retained throughout the process. No other visible reconstructions are found. The width and profile of the LEED spots in Fig. S4, shows the broadening of the LEED spots after the SnO formation on the surface of B-doped C(1 0 0)-(1 × 1):O diamond. This, in our opinion, confirms the claim that SnO deposits as nanoclusters that just broaden the diamond (1 0 0) LEED integral spots. The spa-LEED data is reinforced by the geometry optimised structures obtained in case of both QML and HML of Sn on OTD in different configurations. The reconstruction of the diamond (1 0 0) surface or in other words C—C bonding was seen only in a few configurations e.g., in Fig. 1(b) where a carbonyl or ketone bond exists between surface C and O. Sn bonds with the surface O, resulting in the breaking of ketonic or carbonyl bond between surface C and O and formation of C—C bond and hence a 2 × 1 reconstruction. In all the situation where surface O was bonded in ether configuration to surface C, no reconstruction was seen. No reconstruction was seen due to Sn—Sn bonding in case of HML coverage either which could be attributed to the relatively bigger size of Sn and hence a repulsion as mentioned before.

In order to gain a firm understanding of the surface structure and bonding, the difference in the electrostatic potential between OTD and Sn-OTD surfaces in different configurations (i.e., ether and carbonyl) were investigated using DFT calculations. Fig. 3(a) and (b) shows the electrostatic potential at the surface of ether terminated diamond and when QML of Sn is added to it, respectively. A potential difference of 1.4 eV was obtained in this case which corresponds to the binding energy shift (ΔB.E.) of 1.07 eV in the surface C1s obtained experimentally (Fig. 3(c)). This along with the Spa-LEED analysis makes us believe that Sn atoms have assumed a QML or HML coverage on the ether terminated diamond. This might also indicate that Sn bonds weakly to the OTD surface, as has been seen in case of Al also [28], as ether configuration has slightly lower adsorption energy than ketone/carbonyl one. The bond length didn't vary much between different configurations. C—O Mulliken bond populations between 0.64 and 0.77 were obtained which is significantly implies a single bond. Moreover, Mulliken charges on Sn and O atoms indicate ionic bonds between the surface species (Sn and ether oxygen). As we move from QML to HML, the nature of the bond changes from ionic to a covalent one and hence more NEA, which generally happens with increasing the coverage of metal atoms on the diamond surface. HML, in our case, has been seen to give the maximum NEA and the largest adsorption energy.

3.4. Lithium deposition on SnO terminated diamond

Lithium was deposited at room temperature on the SnO terminated diamond. The lithiation of pristine SnO layers, as observed by Pedersen [41] in a theoretical study, results in the formation of stable layered Li_xO

structure and the expelled tin atoms form atomic planes to separate the Li_xO layers [41].

We have found that as soon as the lithium deposits on the SnO terminated surface of diamond, the reduction of SnO occurs in which Li draws the oxygen atoms from SnO and results in expelled Sn atoms and can be seen in the form of metallic peaks in Fig. 4(a) and (b), which confirms the theoretical predictions made by Pedersen [41]. Table 2 sums up the key results of stoichiometry of the key elements involved in the experiments calculated from the relative peak areas which shows the formation of SnO initially on the diamond surface and then Li_2O/SnO_x on the surface of diamond after lithium deposition and annealing. Tin oxide in the last stage includes a defective oxygen stoichiometry likely due to the oxygen deprivation as a result of lithium inclusion which is also seen in Fig. S6.

The formation of the Li_2O/SnO_x junction was facilitated by annealing the sample at 500 °C. The Li_2O oxide peak increases at the expense of the non-stoichiometric component at 530.5 eV; the Sn oxide peak at 531.3 eV decreases which results from the fact that with an increase in temperature, the oxygen atoms are exchanged between Sn and Li. The formation of Li_2O and metallic Sn indicates the possibility of the formation of 2D planes between lithium oxide layers in a multilayer structure as has been shown by Pedersen [41].

3.5. UPS data for Li—O, SnO terminated diamond and Li_2O/SnO_x terminated diamond

He I UPS was performed after every process in order to have an ultra-surface sensitive acquisition and determine the WFs. The WF can be also
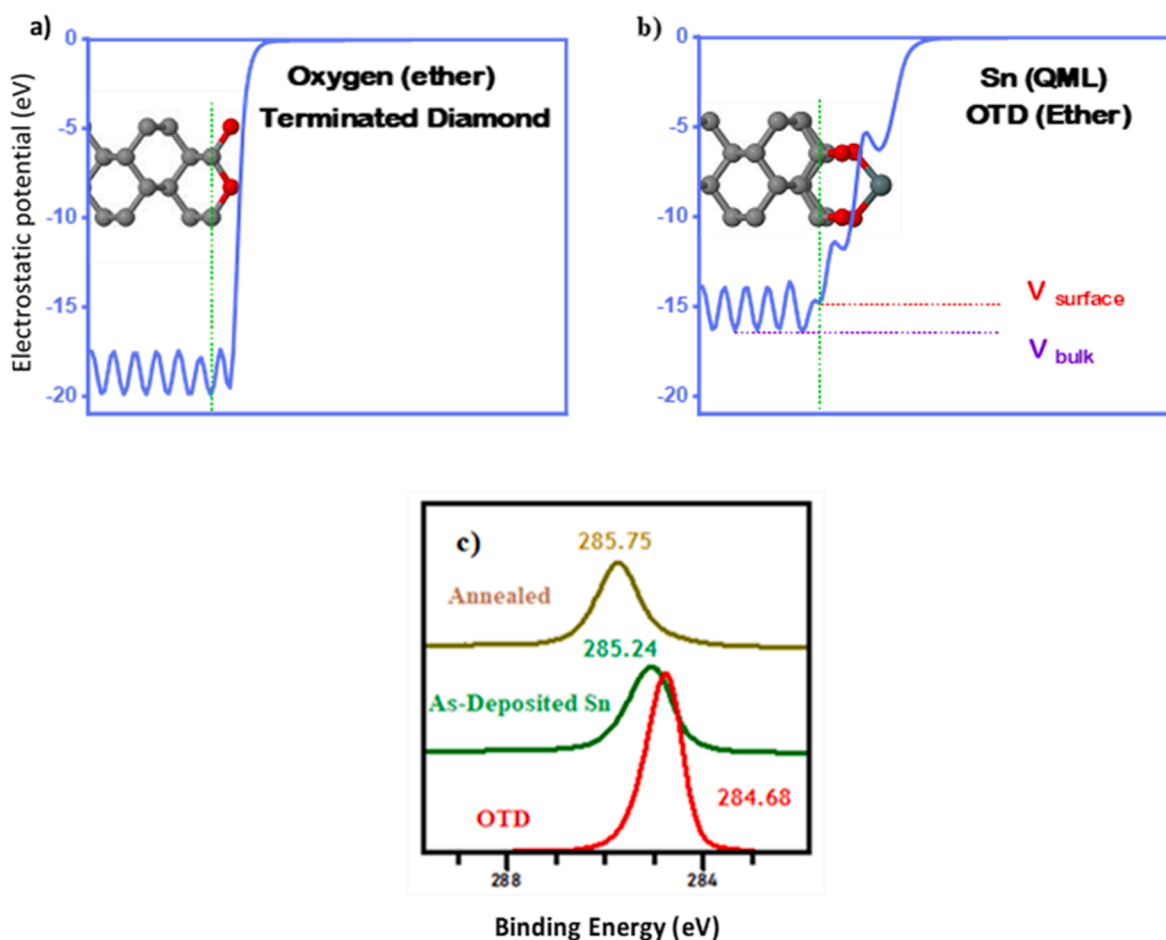

Fig. 3. (a), (b) Electrostatic potential diagram showing variation of potential on the surface of diamond from the bulk diamond in oxygen (ether) terminated diamond and Sn (QML) OTD (ether) terminated diamond, respectively. (c) XPS peaks for surface carbon (C1s) showing the shift in XPS peak.
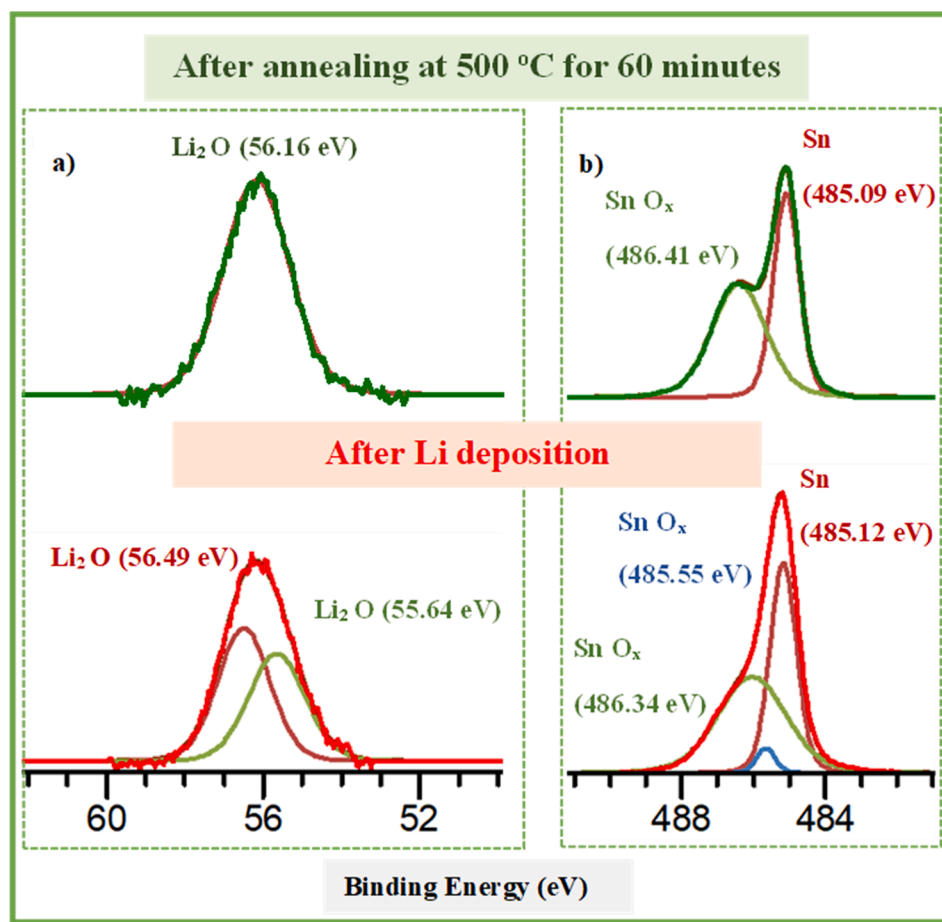
Fig. 4. (a) Lithium peaks (deconvoluted using U 2 Tougaard background and FWHM widths of 1.7 eV ± 0.1 eV for oxide peaks), (b) Sn Peaks (deconvoluted using Shirley background and FWHM of 1.8 eV ± 0.1 eV for oxide peak; As soon as Li was deposited, lithium reduced the tin oxide giving a peak for metallic tin while also giving another peak for lithium oxide. We can also see a clear peak for lithium oxide and SnO after annealing at 500 °C which confirms the formation of Li_2O/SnO_x heterojunction.

Table 2

Summing up the key stoichiometric ratios of the elements involved in the experiment, calculated using the individual peak areas and their corresponding differential photoelectron cross section.

Treatment	Sn:O	Li:O
As deposited Sn	1.25	–
Annealing at 500 °C for 60 min post O cracking	0.82	–
Annealing at 500 °C for 60 min post deposition	3.35	2.35

determined by fitting of EF-PEEM image acquisitions close to the WF threshold (see supporting information Fig. S3). Within our lateral resolution of about 150 nm we found homogenous change in the WF across the sample. The particles on the surface, which broaden the LEED spots (Figs. S4 and S5) are therefore much smaller than our lateral resolution. Fig. S1(f) shows the UPS graphs of the LiO-terminated and Fig. 5 shows SnO and SnO/Li_2O terminated Diamond surface at every step revealing the WF of the material as in the table ST1 in the supplementary section.

Average work functions for various process steps for the Sn 3d and Li 1s spectra are shown in Table ST1. This shows that WF is reduced when Li is deposited and annealed at 500 °C. The annealing further reduces WF by ~0.2 eV due to possible removal of bulk Li as suggested from the XPS. WF reduces from 5.9 eV to 3.93 eV through the surface treatments. At 800 °C, as has been seen in the XPS, much of the oxygen also goes away along with all Li as Li—O resulting in the diamond being almost completely unterminated, hence an increase in the WF. The presence of NEA on LiO terminated diamond has been demonstrated earlier, however in our case it was about −0.60 eV (calculated using Eq. (1) and VBM position from UPS). A discussion on NEA and VBM will be discussed in next section.

In case of SnO_x/Li_2O terminated diamond surfaces, the WF reduces from 5.9 eV to 4.1 eV when only SnO was deposited on the surface of diamond (1 0 0) which is due to the shift in the charge density between the surface species in a way that imparts NEA to the diamond surface as can be shown later. WF is further reduced to 3.9 eV when lithium is deposited on the surface. With an increase in annealing temperature to 500 °C, a WF of 3.6 eV was obtained which is lower than O—Li terminated diamond at that temperature.

This further decrease in WF could be due to the loss of excess lithium during the annealing process as seen in case of O—Li terminated diamond. Furthermore, we have calculated the amount of lithium lost with annealing in both samples and it turned out that 47% of lithium was lost at an annealing temperature of 500 °C for O—Li terminated diamond while only 15% was lost in the case of SnO_x/Li_2O terminated diamond (Fig. S8). This implies towards an increased stability of lithium on the surface of diamond with tin oxide. This is also evidenced by the retention of Li by the sample with tin oxide even at a temperature of 1000 °C, as can be seen in Fig. S8, while Li was totally lost at 800 °C in case of LiO terminated diamond. Another problem with LiO termination of diamond is that Li enters the interstitial sites at higher temperatures which was found earlier [57] and in our study with a different sample as well [59], causing a significant amount of doping and hence upward band bending in the diamond (1 0 0). This band bending can significantly alter the bulk properties of diamond. With SnO terminated diamond, Li is less likely to enter the diamond bulk due to the presence of heavy and large sized Sn atoms present on the surface of diamond. This can be evidenced by a significant amount of downward band bending in our samples with Sn as explained in the next section. This can give more efficient termination of diamond with heterostructures for higher stability and lower WF.
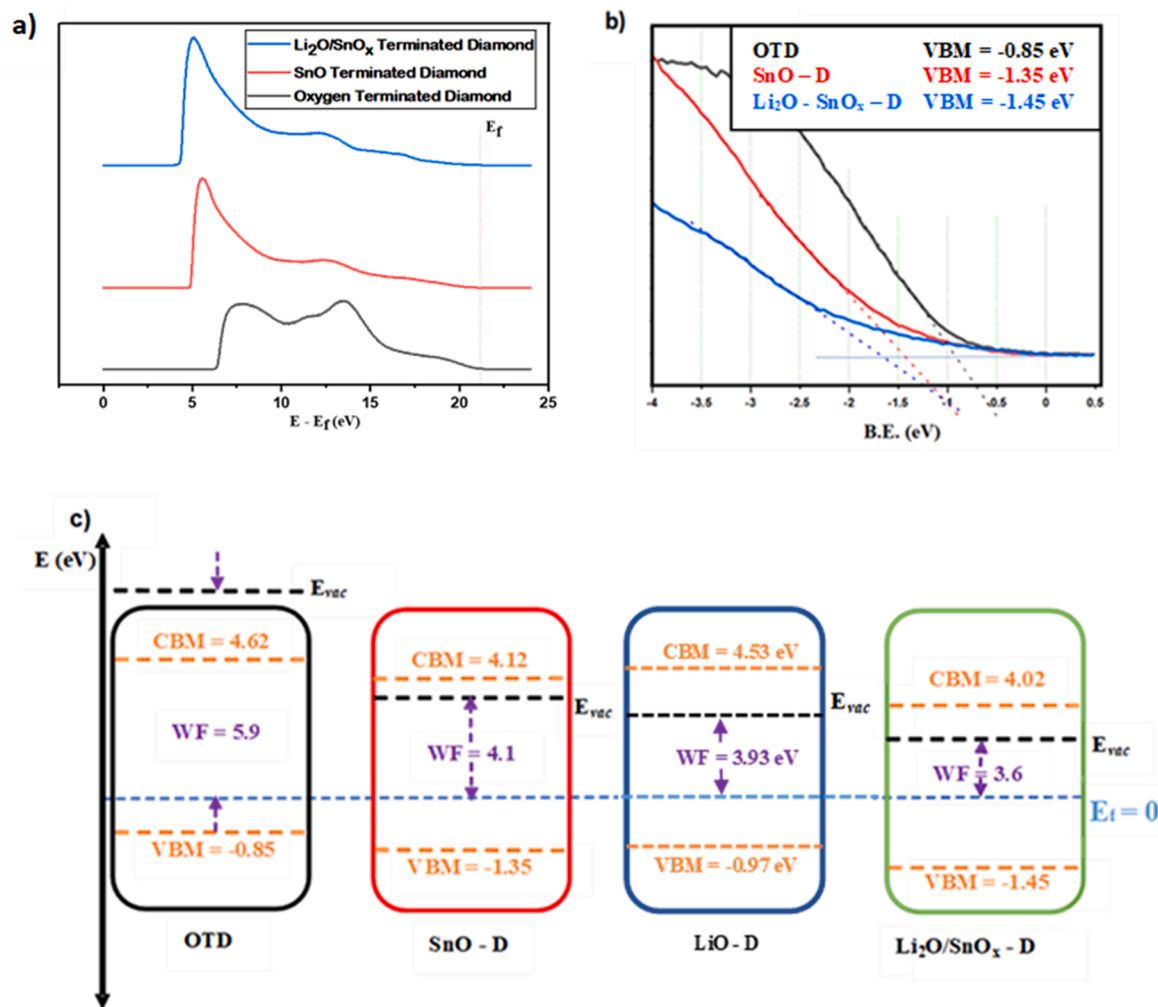
Fig. 5. (a) UPS graphs for LiO-terminated and SnO/Li$_2$O terminated Diamond surface at various process steps. The spectra were produced using a monochromatic 21.2 eV He-I source. WF decreases with the process steps, finally giving a WF reduction of 2.3 eV. (b) VBM position determined using ARPES at 3 process steps. (c) A schematic diagram showing the downward band bending of diamond (1 0 0) due to the various terminations. A band gap of 5.47 eV was assumed in calculating the energy levels.

3.6. Discussion on VBM and NEA

ARPES was done near the top of the valence band to reveal the band structure of the samples and to observe the band bending in the diamond surface due to the metal oxide terminations. However, an increase in the background noise increases the difficulty in visualizing the band structure as can be seen in the supporting information Fig. S2. In spite of this, full wave vector ARPES allowed us to determine the valence band maximum (VBM) position more precisely [8], although it was determined using UPS and Maier 's method [58] also, as can be seen in Fig. S7. The intensity at the centre of ARPES at various steps was plotted against the binding energy (B.E.) which leads to the determination of VBM position at the point where the signal dropped to the background level. The VBM position found due to the above mentioned 3 methods is

presented in Table 3 for comparison with NEA calculated using the equation.

$$\chi = \Phi + \alpha - E_g \tag{1}$$

where χ is electron affinity, Φ is work function (WF), E_g is band gap energy and α is the difference between fermi energy level and VBM. Since the VBM values obtained using full wave vector ARPES are more precise, these were used to calculate the values of NEA.

The electronic structure of differently terminated diamond (1 0 0) is shown in Fig. 5(c) which shows a considerable band bending when LiO, SnO and Li$_2$O-SnO$_x$ is formed on the surface of diamond (1 0 0). VBM position was determined using ARPES (as discussed above), UPS (by extrapolating the low binding energy leading edge of the valence band

Table 3

Electronic structure information at different terminations of diamond (1 0 0). * indicates the values used for calculating the electron affinity (EA) value (by taking their average). VBM was determined using three different methods which showed the same trend. Data for H- terminated diamond is included for comparison.

Sample	VBM (ARPES) (eV)	VBM (UPS) (eV)	Maier's Method (eV)	WF (eV) (±0.1)	EA (eV)	Stability
OTD	0.8*	0.9*	0.75	5.9	1.28 (PEA)	Starts stabilising at 800 °C
HTD [8,10,11]					−1.30 (NEA)	Desorbs at >700 °C
LiO-D	0.9*	1.05*	0.47	3.93	−0.60 (NEA)	Desorbs at 800 °C
SnO-D	1.4*	1.3*	1.75	4.1	−0.02 (NEA)	Desorbs completely at >1000 °C
Li/Sn- OTD	1.5*	1.4*	1.85	3.6	−0.42 (NEA)	Desorbs completely at >1000 °C

linearly into the measured background) (Fig. S7) and by Maier's Method. Although different methods of determining the VBM position gave slightly different values which could be due to errors in the calculation and extrapolation, similar trends in band bending were seen in all the methods. SnO terminated diamond (1 0 0) was seen to have an NEA of −0.02 eV which is less than the theoretically calculated values for QML (−0.86 eV) and HML (−1.37 eV). This could be due to the problems associated with obtaining a smooth and contaminant free surface before metal termination. An increased value of NEA = −0.42 eV is obtained with the lithiation of SnO terminated diamond or in other words with the formation of Li_2O-SnO_x terminated diamond (1 0 0) which calls for improvements to be made in the surface processing steps so that a lower value of NEA and hence WF could be obtained for efficient termination based on a heterostructure between alkali and heavy metals. Although H terminated and LiO terminated diamond surfaces present much higher NEA, however, these terminations desorb at lower temperatures than seen in case of other Sn and heterostructure based terminations.

In order to determine the efficiency in thermionic emission, the UPS spectra results were normalized by the illuminated area and integrated to calculate the quantity of secondary electrons. The integration has been carried out in a zone representative of the secondary electrons. Although O—Li terminated diamond has higher electron yield at every temperature than SnO_x/Li_2O terminated diamond, the decrease in the electrons was more rapid in the former than in the latter sample which also shows the increased stability of Li_2O-SnO_x terminated diamond over the O—Li terminated one. Li termination has already been found to exhibit NEA[51] while the SnO terminated diamond in our study showed a very small value of NEA.

4. Conclusions

We have demonstrated the possibility of forming SnO terminated diamond using DFT calculations. NEA values of −0.86 eV and −1.37 eV were obtained with QML and HML of Sn on oxygen terminated diamond (1 0 0). Larger adsorption energies of more than −6 eV was obtained with various configurations of Sn on OTD which shows that Sn has an ability to form a stable termination on the surface of OTD. This stability was established experimentally as SnO on the surface of diamond was unaffected by molecular oxygen or ambient conditions, a necessary condition for device application. The formation of SnO nano-cluster terminations on the surface of B-doped C(1 0 0)-(1 × 1):O resulted in the downward band bending and lowering of WF by 1.8 eV. An NEA of −0.02 eV was also seen. A considerable amount of downward band bending was seen due to Sn deposition on OTD. SnO was reliably formed instead of SnO_2 which has been a point of debate until now as a reliable reference had been missing. DFT analysis revealed that surface C—C reconstruction due to Sn bonding occurs only in those cases when O atom is bonded to the surface C in a ketone configuration, a larger adsorption and more pronounced NEA was also seen in these cases, which shows Sn prefers to break the ketone bonds than the ether ones. Experimentally, no reconstruction was seen due to SnO termination of diamond.

Although Li—O terminated diamond shows NEA of −0.60 eV with a WF of 3.93 eV, the lithium content decreases quite rapidly at 500 °C. There is also a problem of Li doping the diamond crystal or occupying the interstitial sites inside the diamond bulk and hence changing the bulk properties considerably. The Li interaction with SnO nanoclusters was observed after depositing Li on the SnO terminated diamond. Li withdrew oxygen from the tin oxide and forms Li_2O along with metallic Sn atoms. This interaction resulted in the increased stability of Li on diamond surface. Only about 15% of Li was lost in case of the Li_2O-SnO_x termination on diamond (1 0 0) compared to 47% lost in case of LiO terminated diamond. No surface reconstruction was seen due to Li_2O-SnO_x termination of diamond (1 0 0). By elaboration of the UPS data we also found that the photoelectron yield was decreasing more rapidly in

case of pure LiO compared to Li_2O-SnO_x. Li_2O-SnO_x terminated diamond also resulted in an NEA of −0.42 eV and a WF decrease of 2.3 eV. A downward band bending was seen in case of SnO and Li_2O-SnO_x terminated diamond, as opposed to upward band bending in case of LiO terminated diamond (seen in a different study), which implies that tin oxide can preventing Li from entering the bulk of diamond (doping) and hence preserving the diamond bulk properties.

The results obtained in this study not only provide an insight into the heterostructure termination of diamond but are crucial in developing future efficient terminations for low work-function and NEA on the surface of diamond.

Author contributions

The manuscript was written through contributions of all authors. All authors have given approval to the final version of the manuscript.

CRediT authorship contribution statement

Sami Ullah: Investigation, Methodology, Conceptualization, Software, Visualization, Writing - original draft. **Gary Wan:** Validation, Resources, Writing - review & editing. **Christos Kouzios:** Investigation, Writing - review & editing. **Cameron Woodgate:** Investigation, Validation. **Mattia Cattelan:** Conceptualization, Resources, Data curation, Writing - review & editing. **Neil Fox:** Writing - review & editing, Supervision, Funding acquisition.

Declaration of Competing Interest

The authors declare that they have no known competing financial interests or personal relationships that could have appeared to influence the work reported in this paper.

Appendix A. Supplementary material

Supplementary data to this article can be found online at https://doi.org/10.1016/j.apsusc.2021.149962.

References

[1] G. Xiao, G. Zheng, M. Qiu, Q. Li, D. Li, M. Ni, Thermionic energy conversion for concentrating solar power, Appl. Energy 208 (2017) 1318–1342, https://doi.org/10.1016/j.apenergy.2017.09.021.

[2] F.A.M. Koeck, R.J. Nemanich, Emission characterization from nitrogen-doped diamond with respect to energy conversion, Diam. Relat. Mater. 15 (2–3) (2006) 217–220, https://doi.org/10.1016/j.diamond.2005.08.045.

[3] F.A.M. Koeck, R.J. Nemanich, Advances in Thermionic Energy Conversion through Single-Crystal n-Type Diamond, Front. Mech. Eng. 3 (2017), https://doi.org/10.3389/fmech.2017.00019.

[4] K.M. O'Donnell, et al., Diamond surfaces with air-stable negative electron affinity and giant electron yield enhancement, Adv. Funct. Mater. 23 (45) (2013) 5608–5614, https://doi.org/10.1002/adfm.201301424.

[5] F.A.M. Koeck, R.J. Nemanich, A. Lazea, K. Haenen, Thermionic electron emission from low work-function phosphorus doped diamond films, Diam. Relat. Mater. 18 (5–8) (2009) 789–791, https://doi.org/10.1016/j.diamond.2009.01.024.

[6] "Frontiers | Beta Radiation Enhanced Thermionic Emission from Diamond Thin Films | Mechanical Engineering." https://www.frontiersin.org/articles/10.3389/fmech.2017.00017/full (accessed May 20, 2020).

[7] A. Croot, G. Wan, A. Rowan, H.D. Andrade, J.A. Smith, N.A. Fox, Beta Radiation Enhanced Thermionic Emission from Diamond Thin Films, Front. Mech. Eng. 3 (2017) 17, https://doi.org/10.3389/fmech.2017.00017.

[8] G. Wan, M. Cattelan, N.A. Fox, Electronic structure tunability of diamonds by surface functionalization, J. Phys. Chem. C (2019), https://doi.org/10.1021/acs.jpcc.8b11232.

[9] M.C. James, F. Fogarty, R. Zulkharnay, N.A. Fox, P.W. May, A Review of Surface Functionalisation of Diamond for Thermionic Emission Applications, Carbon (2020), https://doi.org/10.1016/j.carbon.2020.09.019.

[10] J.B. Cui, J. Ristein, M. Stammler, K. Janischowsky, G. Kleber, L. Ley, Hydrogen termination and electron emission from CVD diamond surfaces: A combined secondary electron emission, photoelectron emission microscopy, photoelectron yield, and field emission study, Diam. Relat. Mater. 9 (3) (2000) 1143–1147, https://doi.org/10.1016/S0925-9635(99)00279-4.

[11] D. Takeuchi, S.G. Ri, H. Kato, C.E. Nebel, S. Yamasaki, "Negative electron affinity on hydrogen terminated diamond, Phys. Status Solidi (A) Appl. Mater. Sci. 202 (11) (2005) 2098–2103, https://doi.org/10.1002/pssa.200561927.

[12] F. Maier, M. Riedel, J. Ristein, L. Ley, Origin of Surface Conductivity in Diamond, 2000.

[13] D. Takeuchi, M. Riedel, J. Ristein, L. Ley, Surface band bending and surface conductivity of hydrogenated diamond, Phys. Rev. B - Condens. Matter Mater. Phys. 68 (4) (2003), https://doi.org/10.1103/PhysRevB.68.041304.

[14] K.P. Loh, J.S. Foord, R.G. Egdell, R.B. Jackman, Tuning the electron affinity of CVD diamond with adsorbed caesium and oxygen layers, Diam. Relat. Mater. 6 (5–7) (1997) 874–878, https://doi.org/10.1016/s0925-9635(96)00737-6.

[15] K.P. Loh, X.N. Xie, S.W. Yang, J.S. Pan, P. Wu, A spectroscopic study of the negative electron affinity of cesium oxide-coated diamond (111) and theoretical calculation of the surface density-of-states on oxygenated diamond (111), Diam. Relat. Mater. 11 (7) (2002) 1379–1384, https://doi.org/10.1016/S0925-9635(02)00014-6.

[16] K.W. Wong, Y.M. Wang, S.T. Lee, R.W.M. Kwok, Lowering of work function induced by deposition of ultra-thin rubidium fluoride layer on polycrystalline diamond surface, Appl. Surf. Sci. 140 (1–2) (1999) 144–149, https://doi.org/10.1016/S0169-4332(98)00582-0.

[17] J.L. Nie, H.Y. Xiao, X.T. Zu, F. Gao, First principles calculations on Na and K-adsorbed diamond(1 0 0) surface, Chem. Phys. 326 (2–3) (2006) 308–314, https://doi.org/10.1016/j.chemphys.2006.02.005.

[18] P.K. Baumann, R.J. Nemanich, Characterization of cobalt-diamond (100) interfaces: electron affinity and Schottky barrier, Appl. Surf. Sci. 104–105 (1996) 267–273, https://doi.org/10.1016/S0169-4332(96)00156-0.

[19] P.K. Baumann, R.J. Nemanich, Characterization of copper-diamond (100), (111), and (110) interfaces: Electron affinity and Schottky barrier, Phys. Rev. B 58 (3) (1998) 1643–1654, https://doi.org/10.1103/PhysRevB.58.1643.

[20] P.K. Baumann, R.J. Nemanich, Electron affinity and Schottky barrier height of metal-diamond (100), (111), and (110) interfaces, J. Appl. Phys. 83 (4) (1998) 2072–2082, https://doi.org/10.1063/1.366940.

[21] J. van der Weide, Schottky barrier height and negative electron affinity of titanium on (111) diamond, J. Vac. Sci. Technol. B Microelectron. Nanom. Struct. 10 (4) (1992) 1940, https://doi.org/10.1116/1.586162.

[22] A.K. Tiwari, J.P. Goss, P.R. Briddon, N.G. Wright, A.B. Horsfall, M.J. Rayson, Effect of different surface coverages of transition metals on the electronic and structural properties of diamond, Phys. Status Solidi 209 (9) (2012) 1697–1702, https://doi.org/10.1002/pssa.201200027.

[23] A.K. Tiwari, J.P. Goss, P.R. Briddon, N.G. Wright, A.B. Horsfall, M.J. Rayson, Electronic and structural properties of diamond (001) surfaces terminated by selected transition metals, Phys. Rev. B - Condens. Matter Mater. Phys. 86 (15) (2012), https://doi.org/10.1103/PhysRevB.86.155301.

[24] F.A.M. Köck, J.M. Garguilo, B. Brown, R.J. Nemanich, Enhanced low-temperature thermionic field emission from surface-treated N-doped diamond films, Diam. Relat. Mater. 11 (3–6) (2002) 774–779, https://doi.org/10.1016/S0925-9635(02)00006-7.

[25] S. Petrick, C. Benndorf, Potassium adsorption on hydrogen- and oxygen-terminated diamond(100) surfaces, Diam. Relat. Mater. 10 (3–7) (2001) 519–525, https://doi.org/10.1016/S0925-9635(00)00440-4.

[26] Y. Luo, Comprehensive handbook of chemical bond energies, 2007.

[27] B. Ruscic, D. Feller, K.A. Peterson, Active Thermochemical Tables: dissociation energies of several homonuclear first-row diatomics and related thermochemical values, 2015, pp. 191–202.

[28] M.C. James, A. Croot, P.W. May, N.L. Allan, Negative electron affinity from aluminium on the diamond (1 0 0) surface: A theoretical study, J. Phys. Condens. Matter 30 (23) (2018) 235002, https://doi.org/10.1088/1361-648X/aac041.

[29] K.M. O'Donnell, et al., Diamond Surfaces with Air-Stable Negative Electron Affinity and Giant Electron Yield Enhancement, Adv. Funct. Mater. 23 (45) (Dec. 2013) 5608–5614, https://doi.org/10.1002/adfm.201301424.

[30] A. Schenk, et al., Formation of a silicon terminated (100) diamond surface, Appl. Phys. Lett. 106 (19) (2015), https://doi.org/10.1063/1.4921181.

[31] A.K. Schenk, et al., The surface electronic structure of silicon terminated (100) diamond, Nanotechnology 27 (27) (2016), 275201, https://doi.org/10.1088/0957-4484/27/27/275201.

[32] M.J. Sear, et al., Germanium terminated (1 0 0) diamond, J. Phys. Condens. Matter 29 (14) (2017), 145002, https://doi.org/10.1088/1361-648X/aa57c4.

[33] W. Zhou, N. Umezawa, Band gap engineering of bulk and nanosheet SnO: An insight into the interlayer Sn-Sn lone pair interactions, Phys. Chem. Chem. Phys. 17 (27) (2015) 17816–17820, https://doi.org/10.1039/c5cp02255j.

[34] J. Geurts, S. Rau, W. Richter, F.J. Schmitte, SnO films and their oxidation to SnO2: Raman scattering, IR reflectivity and X-ray diffraction studies, Thin Solid Films 121 (3) (1984) 217–225, https://doi.org/10.1016/0040-6090(84)90303-1.

[35] B.B. Alchagirov, R.K. Arkhestov, F.F. Dyshekova, Electron work function in alloys with alkali metals, Tech. Phys. 57 (11) (2012) 1541–1546, https://doi.org/10.1134/S1063784212110023.

[36] K.J. Saji, K. Tian, M. Snure, A. Tiwari, 2D Tin Monoxide—An Unexplored p-Type van der Waals Semiconductor: Material Characteristics and Field Effect Transistors, Adv. Electron. Mater. 2 (4) (2016) 1–9, https://doi.org/10.1002/aelm.201500453.

[37] A.K. Geim, I.V. Grigorieva, Van der Waals heterostructures, Nature 499 (7459) (2013) 419–425, https://doi.org/10.1038/nature12385.

[38] K.E. Aifantis, S. Brutti, S.A. Hackney, T. Sarakonsri, B. Scrosati, SnO2/C nanocomposites as anodes in secondary Li-ion batteries, Electrochim. Acta 55 (18) (2010) 5071–5076, https://doi.org/10.1016/j.electacta.2010.03.083.

[39] L. Zhang, et al., Low Interface Energies Tune the Electrochemical Reversibility of Tin Oxide Composite Nanoframes as Lithium-Ion Battery Anodes, ACS Appl. Mater. Interfaces 10 (43) (2018) 36892–36901, https://doi.org/10.1021/acsami.8b11062.

[40] W. Dong, et al., A Robust and Conductive Black Tin Oxide Nanostructure Makes Efficient Lithium-Ion Batteries Possible, Adv. Mater. 29 (24) (2017), https://doi.org/10.1002/adma.201700136.

[41] A. Pedersen, M. Luisier, Lithiation of Tin Oxide: A Computational Study, ACS Appl. Mater. Interfaces 6 (24) (2014) 22257–22263, https://doi.org/10.1021/am506108s.

[42] J.P. Perdew, K. Burke, M. Ernzerhof, Generalized gradient approximation made simple, Phys. Rev. Lett. 77 (18) (1996) 3865–3868, https://doi.org/10.1103/PhysRevLett.77.3865.

[43] S.J. Clark, et al., First principles methods using CASTEP, Zeitschrift fur Krist. 220 (5–6) (2005) 567–570, https://doi.org/10.1524/zkri.220.5.567.65075.

[44] D. Vanderbilt, Soft self-consistent pseudopotentials in a generalized eigenvalue formalism, Phys. Rev. B 41 (11) (1990) 7892–7895, https://doi.org/10.1103/PhysRevB.41.7892.

[45] H.J. Monkhorst, J.D. Pack, Special points for Brillouin-zone integrations, Phys. Rev. B 13 (12) (1976) 5188–5192, https://doi.org/10.1103/PhysRevB.13.5188.

[46] S.C. Halliwell, P.W. May, N.A. Fox, M.Z. Othman, Investigations of the co-doping of boron and lithium into CVD diamond thin films, Diam. Relat. Mater. 76 (2017) 115–122, https://doi.org/10.1016/j.diamond.2017.05.001.

[47] J.J. Lander, J. Morrison, Low energy electron diffraction study of the (111) diamond surface, Surf. Sci. 4 (3) (1966) 241–246, https://doi.org/10.1016/0039-6028(66)90004-5.

[48] K.M. O'Donnell, T.L. Martin, N.A. Fox, D. Cherns, The Li-adsorbed C(100)-(1x1): O diamond surface, Mater. Res. Society Symp. Proc. 1282 (2011) 163–168, https://doi.org/10.1557/opl.2011.442.

[49] P.E. Pehrsson, T.W. Mercer, Oxidation of the hydrogenated diamond (100) surface, Surf. Sci. 460 (1–3) (2000) 49–66, https://doi.org/10.1016/S0039-6028(00)00494-5.

[50] J.P. Contour, A. Salesse, M. Froment, M. Garreau, J. Thevenin, "No Title," J. Microsc. Spectrosc. Electron. 4, p. 483.

[51] K.M. O'Donnell, et al., Photoelectron emission from lithiated diamond, Phys. Status Solidi Appl. Mater. Sci. 211 (10) (2014) 2209–2222, https://doi.org/10.1002/pssa.201431414.

[52] "Core level binding energies for the elements Zr-Te (Z=40-52) – IOP science." https://iopscience.iop.org/article/10.1088/0022-3719/13/11/008/pdf (accessed Jun. 06, 2020).

[53] D. Shuttleworth, Preparation of metal-polymer dispersions by plasma techniques. An ESCA investigation, J. Phys. Chem. 84 (12) (1980) 1629–1634, https://doi.org/10.1021/j100449a038.

[54] J. Zheng, et al., From novel PtSn/Pt(110) surface alloys to SnOx/Pt(110) nano-oxides, Surf. Sci. 615 (2013) 103–109, https://doi.org/10.1016/J.SUSC.2013.05.004.

[55] B.E. Park, J. Park, S. Lee, S. Lee, W.H. Kim, H. Kim, Phase-controlled synthesis of SnO x thin films by atomic layer deposition and post-treatment, Appl. Surf. Sci. 480 (2019) 472–477, https://doi.org/10.1016/j.apsusc.2019.03.013.

[56] N.V. Petrova, I.N. Yakovkin, DFT calculations of the electronic structure of SnOx layers on Pd(110), Eur. Phys. J. B 86 (7) (2013), https://doi.org/10.1140/epjb/e2013-40105-5.

[57] M.Z. Othman, P.W. May, N.A. Fox, P.J. Heard, Incorporation of lithium and nitrogen into CVD diamond thin films, Diam. Relat. Mater. 44 (2014) 1–7, https://doi.org/10.1016/J.DIAMOND.2014.02.001.

[58] L. Maier, F. Ristein, J. Ley, Electron affinity of plasma-hydrogenated and chemically oxidized diamond (100) surfaces, Phys. Rev. B 64 (16) (2001), 165411.

[59] Sami Ullah, et al., An investigation into the surface termination and near-surface bulk doping of oxygen-terminated diamond with lithium at various annealing temperatures, MRS Adv. (2021), https://doi.org/10.1557/s43580-021-00060-x. https://rdcu.be/cjKcB.